

Synchronization of Active Atomic Clocks via Quantum and Classical Channels

Alexander Roth* and Klemens Hammerer

*Institute for Theoretical Physics, Institute for Gravitational Physics (Albert Einstein Institute),
Leibniz University Hannover, Callinstraße 38, 30167 Hannover, Germany*

(Dated: May 4, 2022)

Superradiant lasers based on atomic ensembles exhibiting ultra-narrow optical transitions can emit light of unprecedented spectral purity and may serve as active atomic clocks. We consider two frequency-detuned active atomic clocks, which are coupled in a cascaded setup, i.e. as master & slave lasers, and study the synchronization of the slave to the master clock. In a setup where both atomic ensembles are coupled to a common cavity mode such synchronization phenomena have been predicted by Xu et al. [Phys. Rev. Lett. **113**, 154101 (2014)] and experimentally observed by Weiner et al. [arXiv:1503.06464 (2015)]. Here we demonstrate that synchronization still occurs in cascaded setups but exhibits distinctly different phase diagrams. We study the characteristics of synchronization in comparison to the case of coupling through a common cavity. We also consider synchronization through a classical channel where light of the master laser is measured phase sensitively and the slave laser is injection locked by feedback and compare to the results achievable by coupling through quantum channels.

I. INTRODUCTION

Atomic clocks based on optical transitions already achieve record precisions with fractional uncertainties of 10^{-18} [1] and offer great potential for further improvements [2]. Notably, current optical clocks are limited in precision by the instability of the laser used for interrogating the atomic reference system rather than by the linewidth of the clock transition [3]. In order to overcome this limitation the concept of an active atomic clock has been suggested where a lattice of cold atoms with ultra-narrow clock transition itself serves as a laser gain medium resulting in radiation with extremely narrow linewidth in the mHz regime [4–8]. This would remedy the need to reference an external laser to an atomic clock transition.

An active clock laser operates in regime with inverted timescales as compared to a normal laser [4]: In the usual case atoms are pumped incoherently faster than the laser cavity decays. The cavity amplitude then amplifies through stimulated emission only those frequencies which fit within the cavity linewidth. In an active clock laser the atoms are pumped incoherently much slower than the cavity decays. Due to the long lifetime of atomic coherences correlations between the atoms build up giving to a collectively enhanced, superradiant emission into the cavity. The correlations between the atoms result in a linewidth of the output light which is on the order of the one of the atomic transition itself.

Such a superradiant laser exhibits further remarkable properties: Recently it was shown by Xu et al. [9] and experimentally demonstrated by Weiner et al. [10] that two frequency-detuned atom-ensembles coupling to the same cavity mode operated in the superradiant regime synchronize in a large parameter regime; they radiate at the

mean frequency while preserving the narrow linewidth. For larger detuning the ensembles will cross through a phase transition separating the synchronized from the unsynchronized phase and then behave like two independent superradiant lasers at their natural frequency. The synchronization dynamics of superradiant lasers serving as active atomic clocks receives particular importance in the perspective of quantum networks of atomic clocks as envisioned in [11] for enhanced positioning, navigation and geodesy. However, the results of [9, 10] cannot be directly applied to the context of synchronization of remote atomic clocks as the two atomic ensembles are coupled to a common cavity mode.

In the present work we extend the analysis of [9] and consider two remote superradiant lasers coupled through an optical channel in the cascaded configuration of a master and a slave laser. We determine the phase diagram of synchronization in a cascaded setup and determine the parallels and differences to the case of a setup with symmetric coupling studied in [9, 10]. In short, our findings are: synchronization still occurs in a cascaded configuration but the common frequency will always be the one of the master laser in this case. Furthermore, for symmetric coupling the two ensembles in the synchronized phase radiate as one ensemble with $2N$ atoms. This does not occur so in the cascaded setup resulting in changes in the synchronization phase diagram. In either case the linewidth of radiation is the same.

The synchronization of quantum systems has been the subject of several theoretical studies lately [12–16]. Despite these efforts there is no clear measure to distinguish genuine *quantum* synchronization of quantum systems and from a *classical* synchronization of quantum systems. In order to compare the two scenarios in the present context we further extend our analysis and consider toy models where the two lasers are locked to each other through a classical channel, that is, a measurement and feedback procedure. We study both cascaded and symmetric couplings through (idealized) classical channels and compare

* alexander.roth@itp.uni-hannover.de

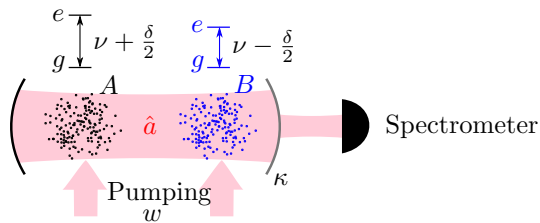


FIG. 1. Two ensembles of two level systems (A and B) coupling to the same cavity mode \hat{a} , as considered in [9]. The frequencies of the transitions $|g\rangle \leftrightarrow |e\rangle$ are detuned by $\pm\delta/2$ from the cavity resonance at frequency ν for ensemble A and B respectively. Atoms are pumped incoherently from $|g\rangle$ to $|e\rangle$ via a third fast decaying level (not shown in level scheme) at rate w and decay from $|e\rangle$ to $|g\rangle$ predominantly through the cavity. The cavity decays at rate κ .

to the results achieved through a quantum channel. In particular we discuss the impact on the linewidth.

The article is organized as indicated in the following table:

	Symmetric coupling	Cascaded setup
Quantum channel	Review of [9], Sec. II A	Sec. II B
Classical channel	Sec. III B	Sec. III A

II. SYNCHRONIZATION THROUGH QUANTUM CHANNELS

A. Synchronization of Two Atomic Ensembles in a Common Cavity

In this section we will briefly review the setup, methods, and results of Xu et al. [9]. We aim to present a sufficient level of detail in order to provide a self-contained derivation of the results going beyond the work of Xu et al. in the later sections. For more details we refer to the excellent presentation in [9]. The setup in Fig. 1 consists of two ensembles of atoms A and B , each containing N atoms, placed in the same cavity. Atoms are assumed to have two relevant internal levels $|g\rangle$ and $|e\rangle$. The transition frequencies of atoms in ensemble A and B have a relative frequency detuning of δ while all atoms within each ensemble are assumed to be frequency degenerate. The transition $|g\rangle \leftrightarrow |e\rangle$ couples to the cavity mode \hat{a} with a single photon Rabi frequency $\Omega/2$. Ensemble A is detuned from the cavity resonance by $\delta/2$ and ensemble B by $-\delta/2$. The cavity linewidth is κ , and we will ultimately assume the bad cavity limit such that the assumptions regarding the detuning of atoms from cavity resonance are insignificant. Atoms decay from $|e\rangle$ to $|g\rangle$ into free space with rate γ_s and dephase with rate T_2^{-1} , and at the same time they are incoherently repumped from $|g\rangle$ to $|e\rangle$ with the rate w (e.g. through an already eliminated third level). In a rotating frame at the cavity frequency the system is described by the Lindblad master

equation

$$\dot{\rho} = -i \left[\frac{\delta}{2} (\hat{J}_A^z - \hat{J}_B^z) + \frac{\Omega}{2} (\hat{a}^\dagger (\hat{J}_A^- + \hat{J}_B^-) + \text{h.c.}) \right] \rho + \kappa \mathcal{D}[\hat{a}] \rho + \sum_{\substack{T=A,B \\ j=1 \dots N}} (\gamma_s \mathcal{D}[\hat{\sigma}_{T,j}^-] + w \mathcal{D}[\hat{\sigma}_{T,j}^+]) \rho. \quad (1)$$

$\hat{\sigma}_{T,j}^z$ and $\hat{\sigma}_{T,j}^\pm$ are the usual Pauli matrices for the $|g\rangle \leftrightarrow |e\rangle$ transition for atom $j \in \{1 \dots N\}$ in ensemble $T \in \{A, B\}$. We use the collective spin operators $\hat{J}_T^\pm := \sum_{i=1}^N \hat{\sigma}_{T,i}^\pm$, $\hat{J}_T^z := \frac{1}{2} \sum_{i=1}^N \hat{\sigma}_{T,i}^z$, and the Lindblad superoperator $\mathcal{D}[A] \rho := A \rho A^\dagger - \frac{1}{2} [A^\dagger A, \rho]_+$. Steady state superradiance is achieved with a dominating cavity decay $\kappa \gg w$, which is inverted compared to an ordinary laser where the pumping dominates $w \gg \kappa$. The fast decay of the cavity with rate κ compared to all other timescales in the system allows for an adiabatic elimination of the cavity mode

$$\hat{a} \simeq -\frac{i\Omega}{\kappa + i\delta} \hat{J}_A^- - \frac{i\Omega}{\kappa - i\delta} \hat{J}_B^- \approx -\frac{i\Omega}{\kappa} (\hat{J}_A^- + \hat{J}_B^-), \quad (2)$$

where we used the approximation that the detuning $\delta \ll \kappa$ is small compared to the cavity linewidth. After adiabatic elimination the decay of the cavity $\kappa \mathcal{D}[\hat{a}] \rho$ translates to a collective decay of the atoms $\gamma \mathcal{D}[\hat{J}^-] \rho$ at rate $\gamma = \Omega^2/\kappa$. The decay into the cavity mode is enhanced by a factor of N and dominates the decay process [5], i.e. $\gamma N \gg \gamma_s, T_2^{-1}$, allowing us to drop the emission into free space and the dephasing

$$\dot{\rho} = -\frac{i\delta}{2} [\hat{J}_A^z - \hat{J}_B^z, \rho] + \gamma \mathcal{D}[\hat{J}_A^- + \hat{J}_B^-] \rho + \sum_{\substack{T=A,B \\ j=1 \dots N}} w \mathcal{D}[\hat{\sigma}_{T,j}^+] \rho. \quad (3)$$

This dynamics can be solved in a mean field approximation with respect to the mean polarization of atoms along z , as developed in Refs. [9] and [4, 5]. Due to the symmetry of (3) all expectation values of Pauli operators must be symmetric under exchange of the particles in each ensemble. Additionally, the differential equations of the expectation values involving only one ensemble are independent of δ and therefore identical for both ensembles, allowing us to drop unnecessary indices $\langle \hat{\sigma}^{\pm,z} \rangle = \langle \hat{\sigma}_{A,i}^{\pm,z} \rangle$, $\langle \hat{\sigma}_1^+ \hat{\sigma}_2^- \rangle = \langle \hat{\sigma}_{A,i}^+ \hat{\sigma}_{A,j}^- \rangle = \langle \hat{\sigma}_{B,i}^+ \hat{\sigma}_{B,j}^- \rangle \forall i \neq j$ and $\langle \hat{\sigma}_A^+ \hat{\sigma}_B^- \rangle = \langle \hat{\sigma}_{A,n}^+ \hat{\sigma}_{B,m}^- \rangle \forall n, m$. Exploiting the symmetry of the master equation it holds $\langle \hat{\sigma}_{T,i}^\pm \rangle = 0$. In order to arrive at a closed set of differential equations third order cumulants are set to zero [5, 9] factorizing third order moments into first and second order moments. Additionally we approximate $\langle \hat{\sigma}_{A,1}^z \hat{\sigma}_{A,2}^z \rangle \approx \langle \hat{\sigma}^z \rangle^2$, which holds true outside of the regime of very weak pumping $w < \gamma, T_2^{-1}, \gamma_s$ [9]. The mean polarization in stationary state in leading order

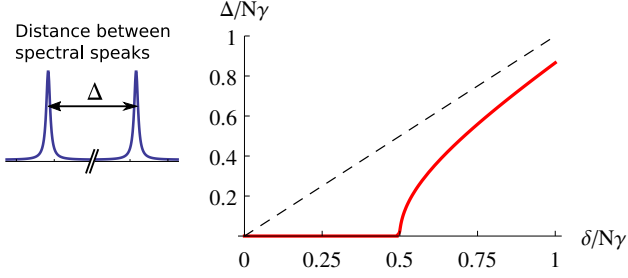


FIG. 2. Effective detuning Δ between the spectral peaks of light emerging from the laser cavity versus detuning δ between the bare transition frequencies of the two ensembles. For $\delta < w$, the rate of incoherent pumping of atoms, the two peaks coalesce signifying synchronization of atoms. The dashed line is $\Delta = \delta$ and is approached asymptotically for $\delta \gg w$.

der $1/N$ is found to be

$$\langle \hat{\sigma}^z \rangle = \begin{cases} \min\left(\frac{w^2 + \delta^2}{2wN\gamma}, 1\right), & 0 \leq \delta < w \\ \min\left(\frac{w}{N\gamma}, 1\right), & \delta \geq w \end{cases}. \quad (4)$$

The synchronization of the two ensembles is witnessed by the spectrum of light emitted from the cavity which is given by the Fourier transform of the two-time correlation function $\langle \hat{a}^\dagger(\tau)\hat{a}(0) \rangle$ of the intra-cavity field. In view of Eq. (2) this requires evaluation of the two-time correlations of atomic dipoles, which can be done by means of the quantum regression theorem. For later reference we explicitly state the corresponding equations of motion for atomic two-time correlation functions,

$$\frac{d}{d\tau} \begin{pmatrix} \langle \hat{\sigma}_A^+(\tau)\hat{\sigma}_B^-(0) \rangle \\ \langle \hat{\sigma}_1^+(\tau)\hat{\sigma}_2^-(0) \rangle \end{pmatrix} = \frac{1}{2} \begin{pmatrix} X & Y \\ Y & X^* \end{pmatrix} \begin{pmatrix} \langle \hat{\sigma}_A^+(\tau)\hat{\sigma}_B^-(0) \rangle \\ \langle \hat{\sigma}_1^+(\tau)\hat{\sigma}_2^-(0) \rangle \end{pmatrix} \quad (5)$$

where $X = \gamma(N-1)\langle \hat{\sigma}^z \rangle - \gamma - w + i\delta$, and $Y = N\gamma\langle \hat{\sigma}^z \rangle$, cf. Eq. (8) in [9]. The two-time correlation functions, the solution of (5), consists of linear combinations of $\exp(-(\Gamma_0 \pm x_0)\tau/2)$, where $\Gamma_0 := w - \gamma(N-1)\langle \hat{\sigma}^z \rangle + \gamma$, and $x_0 := \sqrt{(N\gamma\langle \hat{\sigma}^z \rangle)^2 - \delta^2}$. For $\delta \gg w$ this corresponds to two components oscillating at frequencies $\pm\delta/2$ and decaying at rate Γ_0 . The spectrum thus consists of two separate peaks of width Γ_0 at the bare transitions frequency $\nu \pm \delta/2$ of each ensemble. For smaller detuning δ the coupled dynamics of the two ensembles of atoms first exhibits frequency pulling giving rise an effective detuning $\Delta < \delta$ between the two peaks as long as $\delta > w$, cf. Fig. 2. For $\delta < w$ the two peaks merge and the two ensembles radiate at the same frequency signifying synchronization. The corresponding widths are given by

$$\Gamma/\gamma = \begin{cases} \frac{w^2 + \delta^2}{2wN\gamma} + 1, & 0 \leq \delta < w \\ \frac{w}{N\gamma} + 1, & \delta \geq w \end{cases} \quad (6)$$

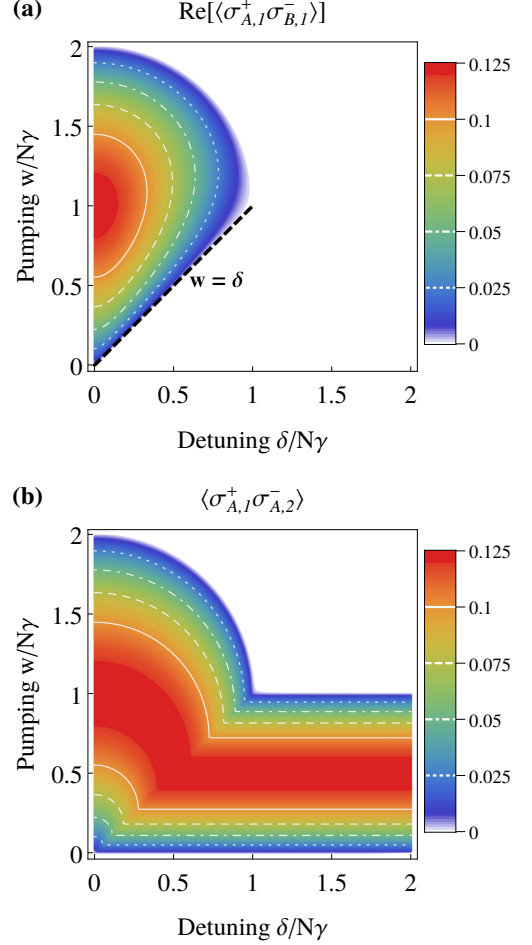


FIG. 3. (a) Non-vanishing inter-ensemble correlations $\text{Re}[\langle \hat{\sigma}_{A,1}^+ \hat{\sigma}_{B,1}^- \rangle]$ outline the synchronized parameter regime. The dashed line $w = \delta$ separates the synchronized from the unsynchronized superradiant regime. (b) shows the inner-ensemble correlations $\langle \hat{\sigma}_1^+ \hat{\sigma}_2^- \rangle$ equal for both ensembles. For detuning smaller than the incoherent pumping rate $\delta < w$ both ensembles are synchronized and the critical pumping rate is moved from $w = N\gamma$ for $\delta > w\xi$ to $w = 2N\gamma$ for $\delta = 0$. Both plots use $N\gamma = 10^6 \text{Hz}$.

in the superradiant regime, which is upper bounded by $\langle \hat{\sigma}^z \rangle < 1$ using (4).

Synchronization of the two active atomic clocks physically means that the collective atomic dipoles oscillate in phase. This corresponds to a large non-zero average value of $\langle \vec{\sigma}_A^\perp \cdot \vec{\sigma}_B^\perp \rangle$ where $\sigma_{A(B)}^\perp$ denotes the spin component transverse to the mean polarization along z for ensemble $A(B)$ (each of which is zero on average in steady state, $\langle \sigma_{A(B)}^\perp \rangle = 0$). It is straight forward to check that $\langle \vec{\sigma}_A^\perp \cdot \vec{\sigma}_B^\perp \rangle = 4 \text{Re}[\langle \hat{\sigma}_A^+ \hat{\sigma}_B^- \rangle]$ such that these inter-ensemble correlations can also be directly used as a measure for synchronization [17]. It is instructive to directly look at this quantity in its dependence on the pumping w and the bare detuning δ , see Fig. 3a. The regime of synchronization is clearly visible as the regime of non-vanishing inter-

ensemble correlations. This regime is bounded by $w = \delta$ and the quarter circle $(w - N\gamma)^2 + \delta^2 = (N\gamma)^2$, which can be derived from (4). The synchronization can be understood as nothing else but the transition from two independent superradiant ensembles $\delta \gg w$ to one superradiant ensemble with $2N$ particles for $\delta = 0$. For $\delta \gg w$ the superradiance is visible in non-vanishing inner-ensemble correlations $\langle \hat{\sigma}_1^\perp \cdot \hat{\sigma}_2^\perp \rangle = 4\langle \hat{\sigma}_1^+ \hat{\sigma}_2^- \rangle$ (see Fig. 3b) and their independence in vanishing inter-ensemble correlations. Decreasing δ into the synchronized regime inter-ensemble correlations build up, approaching the inner-ensemble correlations, until $\delta = 0$ where there is no difference between both ensembles and $\langle \hat{\sigma}_A^+ \hat{\sigma}_B^- \rangle = \langle \hat{\sigma}_1^+ \hat{\sigma}_2^- \rangle$. The additional inter-ensemble correlations in the synchronized regime make the the collective spin $\vec{J}_A + \vec{J}_B$ more robust against noise and move the critical pumping rate for the phase transition between superradiant emission and chaotic light to $w = 2N\gamma$ for $\delta = 0$.

The overall photon flux emerging from the cavity is, for large N ,

$$\langle \hat{a}_{\text{out}}^\dagger \hat{a}_{\text{out}} \rangle \approx 2\gamma N^2 (\langle \hat{\sigma}_1^+ \hat{\sigma}_2^- \rangle + \text{Re} [\langle \hat{\sigma}_A^+ \hat{\sigma}_B^- \rangle]),$$

which follows from Eq. (2) and the input-output relation $\hat{a}_{\text{out}} = \hat{a}_{\text{in}} + \sqrt{\kappa} \hat{a}$ [18]. For $\delta = 0$ the photon flux scales proportional to $(2N)^2$, as one would expect of one ensemble with $2N$ atoms, and scales with $2N^2$ for two independent ensembles each with N atoms.

B. Two Atomic Ensembles in Separate Cascaded Cavities

Next we are going to consider an alternative setup where the two atomic ensembles are kept in separate cavities which are coupled unidirectionally: Light emerging from the cavity containing ensemble A is channeled to the second cavity containing ensemble B , but no light of the latter cavity reaches the first one, cf. Fig. 4. This setup is inherently different from the symmetric configuration in the previous section, and it is unclear if or which synchronization behavior still occurs. What is clear is that the properties of light emitted by ensemble A will be completely unaffected by ensemble B downstream. It is therefore advantageous to assume that the transition frequency of atoms in ensemble A is ν and the one of atoms in ensemble B is $\nu - \delta$ as indicated in Fig. 4. The cavity frequencies are assumed to be equal to ν , but this assumption is insignificant in the bad cavity limit.

The dynamics in this setup is described by means of a cascaded systems master equation [18]. In a rotating frame it is given by

$$\begin{aligned} \dot{\rho} = & -i \left[\frac{\Omega}{2} \left(J_A^+ \hat{a} + J_A^- \hat{a}^\dagger + J_B^+ \hat{b} + J_B^- \hat{b}^\dagger \right) - \delta J_B^z, \rho \right] \\ & + w \sum_{\substack{T=A,B \\ i=1\dots N}} \mathcal{D} \left[\hat{\sigma}_{T,i}^+ \right] \rho + \frac{\kappa}{2} \left[\hat{a}^\dagger \hat{b} - \hat{b}^\dagger \hat{a}, \rho \right] + \kappa \mathcal{D} \left[\hat{a} + \hat{b} \right] \rho, \end{aligned} \quad (7)$$

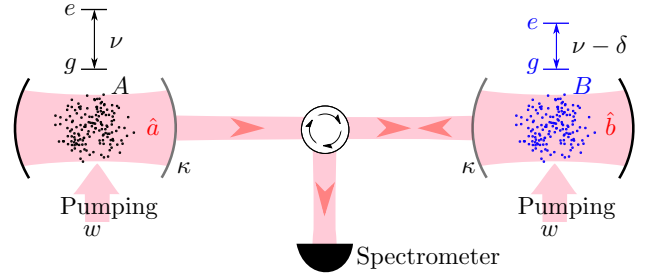


FIG. 4. Two ensembles of two level systems (A and B) coupling to the cavity modes \hat{a}, \hat{b} respectively. The transition frequencies $|g\rangle \leftrightarrow |e\rangle$ of ensemble A and the cavity frequencies \hat{a}, \hat{b} are ν , while ensemble B 's transition frequency is detuned by $-\delta$. Atoms are pumped incoherently from $|g\rangle$ to $|e\rangle$ via a third fast decaying level (not shown in level scheme) at rate w and decay from $|e\rangle$ to $|g\rangle$ predominantly through the cavity. The cavities decay with rate κ and the output of cavity \hat{a} is directly injected into cavity \hat{b} . The output of cavity \hat{b} is diverted into a spectrometer and not into cavity \hat{a} using a lossless Faraday rotator.

The atomic ensembles A and B are coupled to their respective cavity modes \hat{a} and \hat{b} with single-photon Rabi frequency $\Omega/2$, and are pumped incoherently at the rate w to their excited states $|e\rangle$. We dropped already the spontaneous emission into free space and the dephasing, knowing the enhanced decay into the cavity modes \hat{a} and \hat{b} dominate the decay processes, as in the previous section. The last two terms describe the cascaded, unidirectional coupling and decay of the cavity modes at rate κ , cf. [18].

As in section II A the cavity decay is assumed to be the fastest timescale in the system $\kappa \gg \Omega, w$, allowing us to adiabatically eliminate the cavity fields which yields here

$$\hat{a} \simeq \frac{\Omega}{i\kappa} J_A^-, \quad \hat{b} \simeq \frac{\Omega}{i\kappa} (J_B^- - 2J_A^-). \quad (8)$$

The effective master equation for atoms is

$$\begin{aligned} \dot{\rho} = & i\delta [J_B^z, \rho] + w \sum_{T,j} \mathcal{D} \left[\hat{\sigma}_{T,i}^+ \right] \rho \\ & - \frac{\gamma}{2} [J_A^+ J_B^- - J_B^+ J_A^-, \rho] + \gamma \mathcal{D} [J_A^- - J_B^-] \rho \end{aligned} \quad (9)$$

with $\gamma = \Omega^2/\kappa$. Comparing this equation to (3) in the previous section we see that the decay of the two ensembles still happens collectively, despite the relative sign. The additional effective Hamiltonian term describes unidirectional character of the coupling as in Eq. (7).

The master equation implies the following equations of

motion for the expectation values

$$\begin{aligned}
\partial_t \langle \hat{\sigma}_A^z \rangle &= -\langle \hat{\sigma}_A^z \rangle (\gamma + w) - 2\gamma(N-1) \langle \hat{\sigma}_A^+ \hat{\sigma}_A^- \rangle \\
&\quad - \gamma + w \\
\partial_t \langle \hat{\sigma}_A^+ \hat{\sigma}_A^- \rangle &= -\langle \hat{\sigma}_A^+ \hat{\sigma}_A^- \rangle (\gamma + w - \gamma \langle \hat{\sigma}_A^z \rangle (N-2)) \\
&\quad + \frac{\gamma}{2} \langle \hat{\sigma}_A^z \rangle (\langle \hat{\sigma}_A^z \rangle + 1) \\
\partial_t \langle \hat{\sigma}_B^z \rangle &= -\langle \hat{\sigma}_B^z \rangle (\gamma + w) - 2\gamma(N-1) \langle \hat{\sigma}_B^+ \hat{\sigma}_B^- \rangle \\
&\quad - \gamma + w + 4\gamma N \operatorname{Re} [\langle \hat{\sigma}_A^+ \hat{\sigma}_B^- \rangle] \\
\partial_t \langle \hat{\sigma}_B^+ \hat{\sigma}_B^- \rangle &= -\langle \hat{\sigma}_B^+ \hat{\sigma}_B^- \rangle (\gamma + w - \gamma \langle \hat{\sigma}_B^z \rangle (N-2)) \\
&\quad + \frac{\gamma}{2} \langle \hat{\sigma}_B^z \rangle (\langle \hat{\sigma}_B^z \rangle + 1) \\
&\quad - 2\gamma N \langle \hat{\sigma}_B^z \rangle \operatorname{Re} [\langle \hat{\sigma}_A^+ \hat{\sigma}_B^- \rangle] \\
\partial_t \langle \hat{\sigma}_A^+ \hat{\sigma}_B^- \rangle &= \langle \hat{\sigma}_A^+ \hat{\sigma}_B^- \rangle \gamma (N-1) (\langle \hat{\sigma}_A^z \rangle + \langle \hat{\sigma}_B^z \rangle) / 2 \\
&\quad + \langle \hat{\sigma}_A^+ \hat{\sigma}_B^- \rangle (i\delta - \gamma - w) - \frac{\gamma}{2} \langle \hat{\sigma}_B^z \rangle \langle \hat{\sigma}_A^z \rangle \\
&\quad - \frac{\gamma}{2} \langle \hat{\sigma}_B^z \rangle (2\langle \hat{\sigma}_A^+ \hat{\sigma}_A^- \rangle (N-1) + 1), \quad (10)
\end{aligned}$$

where we used the symmetry of (9) to introduce the abbreviations $\langle \hat{\sigma}_A^z \rangle := \langle \hat{\sigma}_{A,i}^z \rangle$, $\langle \hat{\sigma}_B^z \rangle := \langle \hat{\sigma}_{B,i}^z \rangle$, $\langle \hat{\sigma}_A^+ \hat{\sigma}_A^- \rangle = \langle \hat{\sigma}_{A,i}^+ \hat{\sigma}_{A,j}^- \rangle$, $\langle \hat{\sigma}_B^+ \hat{\sigma}_B^- \rangle = \langle \hat{\sigma}_{B,i}^+ \hat{\sigma}_{B,j}^- \rangle$ for $i \neq j$, and $\langle \hat{\sigma}_A^+ \hat{\sigma}_B^- \rangle = \langle \hat{\sigma}_{A,m}^+ \hat{\sigma}_{B,n}^- \rangle$. Note that the symmetry between A and B is broken in the cascaded setup. In (10) we also factorized occurrences of the mean field $\langle \hat{\sigma}_{A(B)}^z \rangle$, which we validated using small system numerical solutions of (7) using QuTiP [19]. The steady state solution can be obtained by setting all time-derivatives on the left hand sides equal to zero and solving the algebraic equations. The first two equations involving only ensemble A can be solved independently of ensemble B , as expected in view of the cascaded setup. The remaining equations can be reduced to a polynomial equation of fourth order, which can be solved exactly and used for analytical results up to leading order in $1/N$. In order to obtain numerical results it is easier and faster to solve the system (10) numerically and select the stable solution by linearizing (10) around each solution.

The spectrum follows again from the Fourier transform of the two-time correlation functions which we calculate using the quantum regression theorem,

$$\frac{d}{d\tau} \begin{pmatrix} \langle \hat{\sigma}_A^+(\tau) \hat{\sigma}_T^-(0) \rangle \\ \langle \hat{\sigma}_B^+(\tau) \hat{\sigma}_T^-(0) \rangle \end{pmatrix} = \frac{1}{2} \begin{pmatrix} X & 0 \\ Y & X' \end{pmatrix} \begin{pmatrix} \langle \hat{\sigma}_A^+(\tau) \hat{\sigma}_T^-(0) \rangle \\ \langle \hat{\sigma}_B^+(\tau) \hat{\sigma}_T^-(0) \rangle \end{pmatrix} \quad (11)$$

with $T = A, B$ and

$$\begin{aligned}
X &= \gamma(N-1) \langle \hat{\sigma}_A^z \rangle - \gamma - w \\
X' &= \gamma(N-1) \langle \hat{\sigma}_B^z \rangle - \gamma - w - 2i\delta \\
Y &= -2N\gamma \langle \hat{\sigma}_B^z \rangle.
\end{aligned}$$

The normalized spectrum of the field emerging from cavity \hat{b} is

$$S_{\text{norm}}(\omega) := \frac{1}{2\pi I} \int d\tau \exp(-i\omega\tau) \langle \hat{b}_{\text{out}}^\dagger(\tau) \hat{b}_{\text{out}}(0) \rangle$$

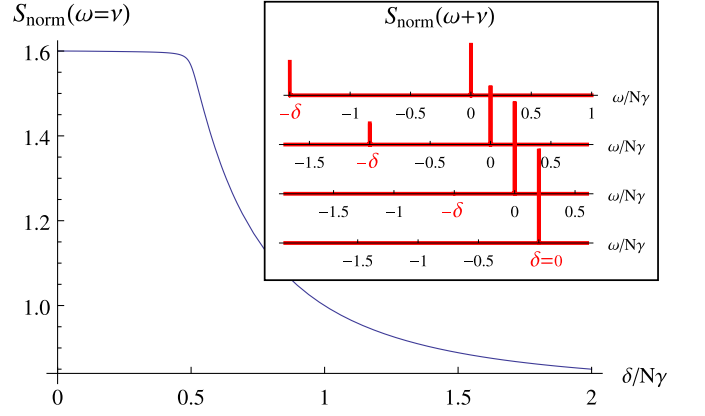


FIG. 5. (Main plot): $S_{\text{norm}}(\omega = \nu)$ is the photon flux at the resonance frequency ν of ensemble A . Since ensemble A is independent of δ any change with δ comes from ensemble B also at frequency ν . For decreasing δ ensemble B radiates stronger on the injected frequency ν and less at its resonance frequency $\nu - \delta$. For $\delta < w$ ensemble B radiates dominantly on the injected frequency ν and decreasing δ further does not change this, resulting in the plateau of $S_{\text{norm}}(\omega = \nu)$. (Inset): The normalized spectrum $S_{\text{norm}}(\omega)$ for multiple detunings $\delta/N\gamma = 1.5, 1, 0.5, 0$ shows a suppression of the peak at $\nu - \delta$ for decreasing detuning δ , while the Lorentz peak at ν rises until ensemble B is radiating dominantly at ν . Both plots use for the parameters $N\gamma = 10$ kHz and $w = 0.5N\gamma$.

which can be evaluated using the input-output relation for cascaded systems [18]

$$\hat{b}_{\text{out}} = \hat{a}_{\text{in}} + \sqrt{\kappa}(\hat{a} + \hat{b}). \quad (12)$$

and Eq. (8). The normalization factor is $I = \langle \hat{b}_{\text{out}}^\dagger \hat{b}_{\text{out}} \rangle$. The peaks in $S_{\text{norm}}(\omega)$ are always located at the bare transition frequencies ν and $\nu - \delta$ of ensemble A and B respectively which does not hint at synchronization effects. Synchronization becomes visible in the regime $\delta < w < N\gamma$ via a change of relative peak heights, as illustrated in Fig. 5 Inset, which is qualitatively different from the frequency pulling in section II A. For fixed pumping w in the superradiant regime [4] $\gamma < w < N\gamma$ we can distinguish different regimes for δ

$\delta \gg w$: Ensembles A and B radiate only at their own resonance frequency $\nu, \nu - \delta$ respectively with equal intensity.

$\delta \geq w$: Ensemble A is unaffected by any change in δ and radiates at ν , but ensemble B radiates at two frequencies ν and $\nu - \delta$. This leads to an increasing total intensity at frequency ν , cf. Fig. 5.

$\delta < w$: Ensemble A still radiates with the same intensity at frequency ν and ensemble B now also dominantly radiates at frequency ν , while radiation at its own resonance frequency becomes negligible (for large N). Ensemble B is synchronized to ensemble A resulting in a plateau of $S_{\text{norm}}(\nu)$, cf. Fig. 5.

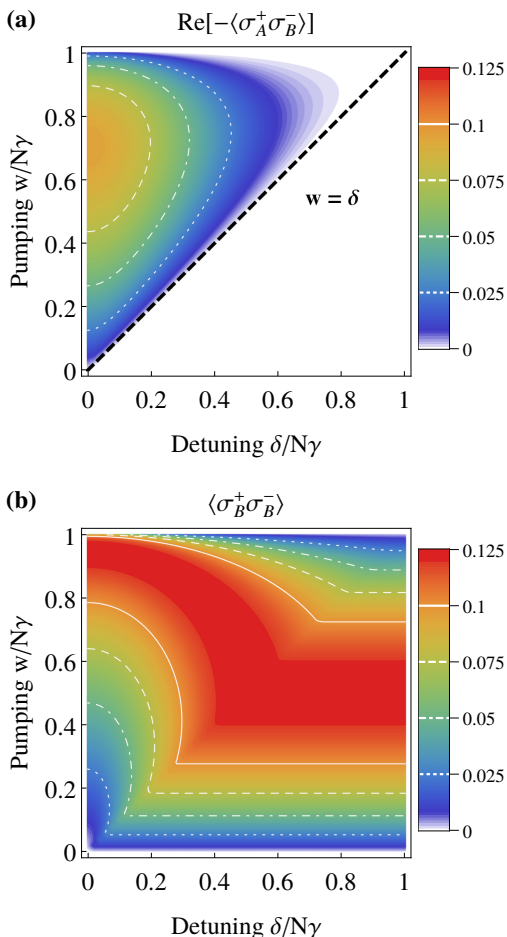


FIG. 6. (a) Non-vanishing inter-ensemble correlations $\text{Re}[-\langle\hat{\sigma}_A^+\hat{\sigma}_B^-\rangle]$ outline the synchronized parameter regime. The dashed line $w = \delta$ separates the synchronized from the unsynchronized superradiant regime. (b) shows the inner-ensemble correlations $\langle\hat{\sigma}_B^+\hat{\sigma}_B^-\rangle$ of the slave ensemble B . For detuning smaller than the incoherent pumping rate $\delta < w$ the slave ensemble B is synchronized to the master ensemble A . Here $N\gamma = 10^6\text{Hz}$.

While the peak value of the normalized spectrum at frequency ν shows a plateau in the synchronized regime $\delta < w$, the integrated unnormalized spectrum, that is the total power output is still increasing for smaller detuning, similar to the finding in section II A. In leading order in N^2 the total photon flux is given by

$$\langle\hat{b}_{\text{out}}^\dagger\hat{b}_{\text{out}}\rangle \approx \gamma N^2 \left(\sum_{T=A,B} \langle\hat{\sigma}_{T,1}^+\hat{\sigma}_{T,2}^-\rangle + 2 \text{Re}[-\langle\hat{\sigma}_A^+\hat{\sigma}_B^-\rangle] \right).$$

The photon flux increases for smaller detuning δ due to increasing correlations $\text{Re}[-\langle\hat{\sigma}_A^+\hat{\sigma}_B^-\rangle]$ between the two ensembles as shown in Fig. 6a. In Section II A the synchronized regime stretched out beyond $w = N\gamma$ up to $w = 2N\gamma$ for vanishing detunings, cf. Fig. 3 due to the fact that the two ensembles radiate in this regime as one ensemble containing $2N$ atoms. This is not the case in

the cascaded system, see Fig. 6. For $w > N\gamma$ ensemble A (containing N atoms) will stop emitting superradiantly and for $w \gg N\gamma$ will radiate chaotic light [5]. The correlations $\langle\hat{\sigma}_B^+\hat{\sigma}_B^-\rangle$ shown in Fig. 6b indicate that if the first cavity would still radiate superradiantly (e.g. N larger in the first cavity), then the synchronized regime could also stretch beyond $w = N\gamma$.

Analyzing the Lorentz peaks in the spectrum reveals that the peaks at ν and $\nu - \delta$ have a width

$$\frac{\Gamma_\nu}{\gamma} = \frac{w}{N\gamma} + 1, \quad (13)$$

$$\frac{\Gamma_{\nu-\delta}}{\gamma} = \begin{cases} O(N), & \delta \leq w \\ \frac{w}{N\gamma} + 1, & \delta > w \end{cases}, \quad (14)$$

which is valid up to order $1/N$ in the superradiant regime. Most significantly we see that the linewidth at $\nu - \delta$ for $\delta \leq w$ scales with N and as a result the peak effectively vanishes for large N . This shows that ensemble B cannot sustain radiating at its resonance frequency and radiates instead at the frequency of ensemble A . The independence of Γ_ν of δ is also significant, since it means that in the synchronized regime ensemble B is amplifying the input signal without increasing the linewidth.

III. SYNCHRONIZATION THROUGH CLASSICAL CHANNELS

A. Unidirectional Synchronization

One can ask the question whether the synchronization in Section II B is dominated by quantum mechanics and requires a quantum channel in between both cavities or whether the same or a similar result can be achieved by synchronizing the two clocks through a classical channel. Synchronization or locking of the two superradiant laser through a classical channel means that classical information is transmitted between the two systems, rather than quantum states of light as was considered in the previous section.

In this section we are going to answer this questions for a highly idealized classical channel: We will consider phase sensitive measurements (heterodyne detection) of the output field of one laser cavity, transmission of the classical measurement result (the photocurrent), and injection of an appropriate coherent field to the second cavity. Thus, we assume a continuous-time feedback strategy where the measured amplitude and phase of the field of the first cavity is recreated with appropriate feedback gains as a seed for the second cavity as illustrated in Fig. 7. This measure and prepare strategy simulates the direct injection of Section II B. Both heterodyne measurement and laser are idealizations adding no technical noise, but will add quantum noise due to the gain of classical information. From a quantum information point

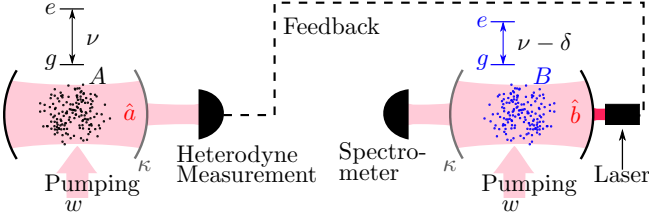


FIG. 7. Two ensembles of two level systems (A and B) coupling to the cavity modes \hat{a}, \hat{b} respectively. The transition frequencies $|g\rangle \leftrightarrow |e\rangle$ of ensemble A and the cavity frequencies \hat{a}, \hat{b} are ν , while ensemble B 's transition frequency is detuned by $-\delta$. Atoms are pumped incoherently from $|g\rangle$ to $|e\rangle$ via a third fast decaying level (not shown in level scheme) at rate w and decay from $|e\rangle$ to $|g\rangle$ predominantly through the cavity. The cavities decay with rate κ and the output of cavity \hat{a} is measured via an ideal heterodyne detection and then recreated with an ideal laser with a certain gain and fed into cavity \hat{b} . The measurement and feedback via the laser are a classical simulation of the direct injection in Section II B.

of view we have replaced the quantum channel between both cavities by a classical channel and local operations. We will show that this introduces a certain level of additional noise due to the measurement, but will not change the synchronization behavior.

This result has to be understood as an upper bound to the quality of classical synchronization achievable through a classical channel. Any real classical procedure will actually perform worse, as it will add technical noise in phase sensitive detection and feedback. This will be especially relevant when attempting to synchronize superradiant lasers exhibiting unprecedentedly low linewidths.

To describe the system we use an unconditional feedback master equation using continuous-time heterodyne measurements developed in [21, 22]

$$\begin{aligned} \dot{\rho} = & -i[H, \rho] - \frac{i}{4} \left[\left(\hat{F}_+ + i\hat{F}_- \right) \hat{s} + h.c., \rho \right] \\ & + \frac{1}{2} \mathcal{D} \left[\hat{s} - i\hat{F}_+ \right] \rho + \frac{1}{2} \mathcal{D} \left[\hat{s} - \hat{F}_- \right] \rho. \end{aligned} \quad (15)$$

The operator \hat{s} describes the type of measurement being performed which, for the case of a heterodyne detection, is given by $\hat{s} = \sqrt{\kappa} \hat{a}$. The heterodyne detection provides two photocurrents I_{\pm} for the phase and the amplitude quadrature which can be used for the feedback operation. We consider Markovian and linear feedback, that is, the photocurrents are each multiplied by suitable gains and, in the case considered here, fed back as a coherent driving field to the second cavity. The feedback due to the two photocurrents I_{\pm} is described by Hermitian operators \hat{F}_{\pm} which are given by $\hat{F}_{\pm} = g_{\pm} \hat{b} + g_{\pm}^* \hat{b}^{\dagger}$ with gain coefficients $g_+ = -i\sqrt{\kappa}$ and $g_- = -\sqrt{\kappa}$. We choose this particular feedback strategy as it reproduces an unidirectional coupling identical to the one found in Eq. (7)

when inserted to the feedback master equation in (15),

$$\begin{aligned} \dot{\rho} = & -i \left[\frac{\Omega}{2} \left(J_A^+ \hat{a} + J_A^- \hat{a}^{\dagger} + J_B^+ \hat{b} + J_B^- \hat{b}^{\dagger} \right) - \delta J_B^z, \rho \right] \\ & + w \sum_{\substack{T=A,B \\ i=1\dots N}} \mathcal{D} \left[\hat{\sigma}_{T,i}^+ \right] \rho + \frac{\kappa}{2} \left[\hat{a}^{\dagger} \hat{b} - h.c., \rho \right] + \kappa \mathcal{D} \left[\hat{a} + \hat{b} \right] \rho \\ & + \kappa \mathcal{D} \left[\hat{b} \right] \rho + \kappa \mathcal{D} \left[\hat{b}^{\dagger} \right] \rho. \end{aligned}$$

We added the incoherent atom pumping with rate w and the decay of cavity field \hat{b} with rate κ . The coherent dynamics is given by the atom-cavity interaction at rate $\Omega/2$, and the detuning of the atomic transitions $-\delta$, as in the previous section. The only difference to (7) are the last to cooling and heating terms indicating additional noise due to the measurement.

The cavity fields can again be adiabatically eliminated considering the subtlety that cavity \hat{b} is now driven with rate κ by the Lindblad terms to a thermal state with 1 mean photon. The adiabatic elimination translates the decays of the cavity modes to a collective decay of the atoms at rate $\gamma = \Omega^2/\kappa$

$$\begin{aligned} \dot{\rho} = & i\delta [J_B^z, \rho] + \gamma \mathcal{D} \left[J_A^- - J_B^- \right] \rho + \frac{\gamma}{2} \left[J_B^+ J_A^- - h.c., \rho \right] \\ & + w \sum_{\substack{T=A,B \\ i=1\dots N}} \mathcal{D} \left[\hat{\sigma}_{T,i}^+ \right] \rho + \gamma \mathcal{D} \left[J_B^- \right] \rho + \gamma \mathcal{D} \left[J_B^+ \right] \rho. \end{aligned}$$

The corresponding dynamics of the expectation values is

$$\begin{aligned} \partial_t \langle \hat{\sigma}_A^z \rangle = & -\langle \hat{\sigma}_A^z \rangle (\gamma + w) - 2\gamma (N-1) \langle \hat{\sigma}_A^+ \hat{\sigma}_A^- \rangle \\ & - \gamma + w \\ \partial_t \langle \hat{\sigma}_A^+ \hat{\sigma}_A^- \rangle = & -\langle \hat{\sigma}_A^+ \hat{\sigma}_A^- \rangle (\gamma + w - \gamma \langle \hat{\sigma}_A^z \rangle (N-2)) \\ & + \frac{\gamma}{2} \langle \hat{\sigma}_A^z \rangle (\langle \hat{\sigma}_A^z \rangle + 1) \\ \partial_t \langle \hat{\sigma}_B^z \rangle = & -\langle \hat{\sigma}_B^z \rangle (\gamma u + w) - 2\gamma (N-1) \langle \hat{\sigma}_B^+ \hat{\sigma}_B^- \rangle \\ & - \gamma + w + 4\gamma N \text{Re} \left[\langle \hat{\sigma}_A^+ \hat{\sigma}_B^- \rangle \right] \\ \partial_t \langle \hat{\sigma}_B^+ \hat{\sigma}_B^- \rangle = & -\langle \hat{\sigma}_B^+ \hat{\sigma}_B^- \rangle (u\gamma + w - \gamma \langle \hat{\sigma}_B^z \rangle (N-2)) \\ & + \frac{\gamma}{2} \langle \hat{\sigma}_B^z \rangle (u \langle \hat{\sigma}_B^z \rangle + 1) \\ & - 2\gamma N \langle \hat{\sigma}_B^z \rangle \text{Re} \left[\langle \hat{\sigma}_A^+ \hat{\sigma}_B^- \rangle \right] \\ \partial_t \langle \hat{\sigma}_A^+ \hat{\sigma}_B^- \rangle = & \langle \hat{\sigma}_A^+ \hat{\sigma}_B^- \rangle \gamma (N-1) (\langle \hat{\sigma}_A^z \rangle + \langle \hat{\sigma}_B^z \rangle) / 2 \\ & + \langle \hat{\sigma}_A^+ \hat{\sigma}_B^- \rangle (i\delta - v\gamma - w) - \frac{\gamma}{2} \langle \hat{\sigma}_B^z \rangle \langle \hat{\sigma}_A^z \rangle \\ & - \frac{\gamma}{2} \langle \hat{\sigma}_B^z \rangle (2\langle \hat{\sigma}_A^+ \hat{\sigma}_A^- \rangle (N-1) + 1), \end{aligned} \quad (16)$$

where $u = 3$ and $v = 2$. This is almost identical to the dynamics found for the cascaded system considered in the previous section, Eqs. (10) and (11), which are identical the set of equations in (16) when the parameters u and v are set to $u = 1$ and $v = 1$. Importantly, u and v never occur multiplied with N, w, δ and therefore do not contribute significantly to the dynamics in the limit of large N . This is also visible in the steady state results in Figs. 8 and showing no visible difference to Fig. 6.

To evaluate if ensemble B synchronizes with ensemble A , just like in Section II B, we extract from the two-time correlation functions the components $\exp(-\Gamma_\nu\tau/2)$ and $\exp(-(\Gamma_{\nu-\delta}/2 + i\delta)\tau)$. Using the solutions for $\langle\hat{\sigma}_A^z\rangle$ and $\langle\hat{\sigma}_B^z\rangle$, which are identical to Section II B up to leading order in $1/N$, we calculate the width of these Lorentzian peaks, giving in the superradiant regime

$$\frac{\Gamma_\nu}{\gamma} = \frac{w}{N\gamma} + 1, \quad \frac{\Gamma_{\nu-\delta}}{\gamma} = \begin{cases} O(N), & \delta \leq w \\ \frac{w}{N\gamma} + 3, & \delta > w \end{cases}.$$

Just as in Section II B we see that the peak at $\nu - \delta$ for $\delta \leq w$ gets extremely broad for large N and thus effectively vanishes. Again this means that the resonance frequency of ensemble B is suppressed and ensemble B synchronizes to the frequency of ensemble A . Remarkable is that even though there is now a classical channel between both cavities, ensemble B amplifies the input signal in the synchronized regime without increasing the linewidth Γ_ν . In the unsynchronized regime $\delta > w$ the linewidth $\Gamma_{\nu-\delta}$ is larger than in the quantum coupled setup (14). Due to the chosen gain in the feedback operators $\hat{F}_\pm = g_\pm\hat{b} + g_\pm^*\hat{b}^\dagger$ the output spectrum of cavity \hat{b} has now a larger Lorentz peak at ν than at $\nu - \delta$ for large detuning $\delta \gg w$. This stronger feedback gain is necessary to simulate the same amplitude of cavity field \hat{a} being injected into cavity \hat{b} as in Sec. II B.

From the dynamics of the expectation values (16) and from the correlation functions in the steady state Fig. 8 we see that there is no significant difference in the synchronization between the quantum and the classically coupled setups considered in the previous and this section, respectively. This holds in the limit of large N , that is far above threshold of the superradiant laser where the emitted field is essentially classical. However, it is important to remember that our analysis is based on an ideal heterodyne detection and feedback operations, and that any realistic classical synchronization will perform worse.

B. Bidirectional Synchronization

In view of the results of the previous section it is worthwhile considering the question whether the synchronization in Section II A was dependent on the coupling to the same quantum mechanical cavity mode, or if this synchronization also occurs when we replace this quantum coupling with a classical, bidirectional coupling. In order to address this question we consider the setup in Fig. 9. Both cavity fields decay with rate $\tilde{\kappa}$ and are measured with ideal heterodyne measurements. The measurement results are then used by an ideal lasers to recreate the measured coherent state with a certain gain, giving rise to a symmetric coupling between both cavities using classical channels. Just like in the previous section are the heterodyne measurements and lasers idealizations adding no technical noise and the continuous-time

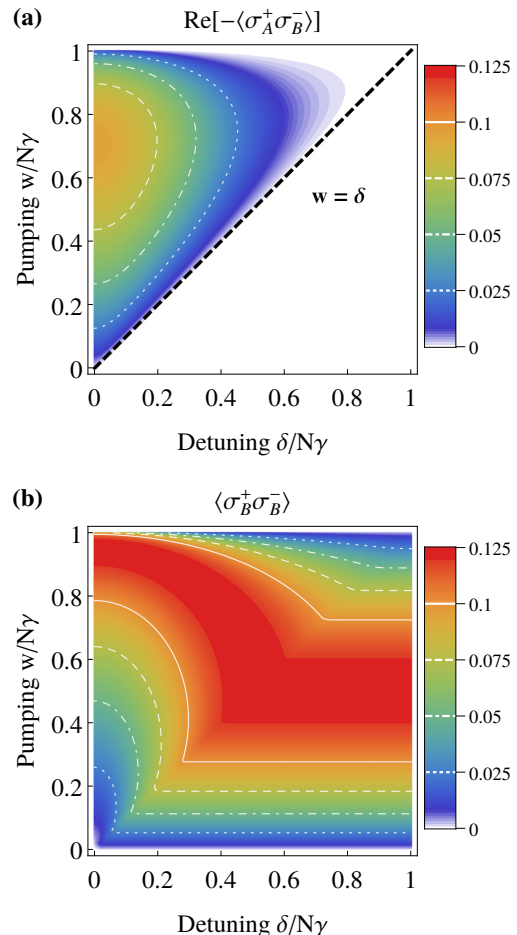


FIG. 8. (a) Non-vanishing inter-ensemble correlations $\text{Re}[-\langle\hat{\sigma}_A^+\hat{\sigma}_B^-\rangle]$ outline the synchronized parameter regime. The dashed line $w = \delta$ separates the synchronized from the unsynchronized superradiant regime and is identical to Sec. II B. (b) shows the inner-ensemble correlations $\langle\hat{\sigma}_B^+\hat{\sigma}_B^-\rangle$ of the slave ensemble B . Here $N\gamma = 10^6\text{Hz}$.

feedback is instantaneous – i.e. Markovian. This setup is a strategy to simulate the coupling to the same cavity mode in Section II A with a classical (but not necessarily technical feasible) bi-directional coupling. In this section we will give a brief overview over our analysis and its results and refer to the Appendix for a complete derivation.

To describe this system we use the same unconditional feedback master equation (15) twice. Once with the measurement operator $\hat{s}_a = \sqrt{\tilde{\kappa}}\hat{a}$ and feedback operators $\hat{F}_\pm^{\hat{b}} = g_\pm\hat{b} + g_\pm^*\hat{b}^\dagger$ acting on field \hat{b} , and then with the measurement operator $\hat{s}_b = \sqrt{\tilde{\kappa}}\hat{b}$ and feedback operator $\hat{F}_\pm^{\hat{a}} = g_\pm\hat{a} + g_\pm^*\hat{a}^\dagger$ acting on field \hat{a} , where $g_+ := g_-/i$. Without loss of generality we can introduce the feedback strength ξ with $g_- := -\xi\sqrt{\tilde{\kappa}}$ and restrict the feedback strength to $\xi \in [0, 1)$, such that the resulting equations form a stable system for the cavity fields. If ξ would be allowed to be equal to unity or larger, the measurement

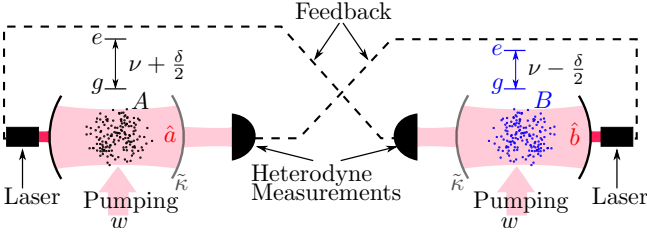


FIG. 9. Two ensembles of two level systems (A and B) coupling to the cavity modes \hat{a}, \hat{b} respectively. The frequencies of the transitions $|g\rangle \leftrightarrow |e\rangle$ are detuned by $\pm\delta/2$ from the cavity resonance at frequency ν for ensemble A and B respectively. Atoms are pumped incoherently from $|g\rangle$ to $|e\rangle$ via a third fast decaying level (not shown in level scheme) at rate w and decay from $|e\rangle$ to $|g\rangle$ predominantly through the cavity. The cavities decay with rate $\tilde{\kappa}$ and the output of both cavities is measured via an ideal heterodyne detection and then recreated with an ideal laser with a certain gain and fed into the opposite cavity. The measurements and feedbacks via the lasers are symmetric such that this simulates the coupling to the same cavity mode as in Sec. II A.

& feedback would increase the amplitude of the cavity fields and there would be no steady state with finite amplitudes. We can proceed with adiabatically eliminating the cavity fields, which gives the master equation for the atoms only

$$\begin{aligned} \dot{\rho} = & \frac{\delta}{2i} [J_A^z - J_B^z, \rho] + \sum_{\substack{T \in \{A, B\} \\ i \in \{1..N\}}} w \mathcal{D} [\hat{\sigma}_{T,i}^+] \rho + \sum_{s=\pm} \frac{\Omega^2}{2\kappa_s} \times \\ & \times \left((1 + \bar{n}_s) \mathcal{D} [J_A^- - sJ_B^-] + \bar{n}_s \mathcal{D} [J_A^+ - sJ_B^+] \right) \rho, \end{aligned} \quad (17)$$

where $\kappa_{\pm} := \tilde{\kappa} (1 \pm \xi)$ and $\bar{n}_{\pm} := \xi^2 / (4(1 \pm \xi))$.

For $\xi = 0$ the second Lindblad terms drop out and the first Lindblad terms can be transformed to show independent decay for both ensembles. For $\xi \neq 0$ the Lindblad terms cannot be separated for both ensembles and for increasing ξ both ensembles couple more and more strongly. Comparing the dynamics of $\langle \hat{\sigma}_A^+ \rangle$ with the completely uncoupled case and the completely coupled case in Sec. II A we choose the cavity decays $\tilde{\kappa}$ dependent on the feedback strength ξ such that both cases are simulated best:

$$\tilde{\kappa}(\xi) := \frac{\kappa}{(1 - \xi)(1 + \xi)}. \quad (18)$$

From master equation (17) with the parameterization (18) we can calculate the dynamics of the expectation

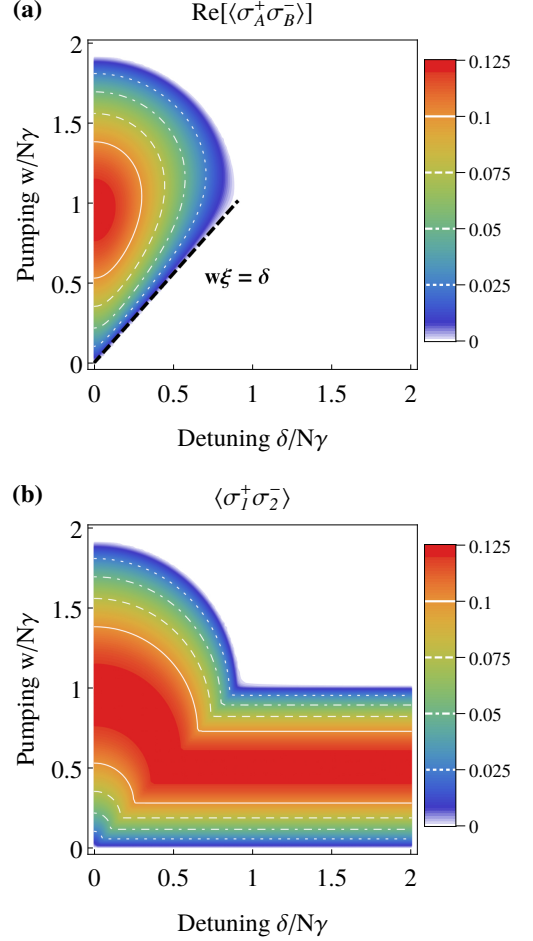


FIG. 10. (a) Non-vanishing inter-ensemble correlations $\text{Re}[\langle \hat{\sigma}_A^+ \hat{\sigma}_B^- \rangle]$ outline the synchronized parameter regime. This regime is reduced compared to Fig. 3, and the dashed line $w\xi = \delta$ separates the synchronized from the unsynchronized superradiant regime. (b) shows the inner-ensemble correlations $\langle \hat{\sigma}_1^+ \hat{\sigma}_2^- \rangle$ equal for both ensembles. For detuning smaller than the incoherent pumping rate times the feedback strength $\delta < w\xi$ both ensembles are synchronized and the critical pumping rate is moved from $w = N\gamma$ for $\delta > w\xi$ to $w = (1 + \xi)N\gamma$ for $\delta = 0$. Both plots use $N\gamma = 10^6 \text{Hz}$.

values

$$\begin{aligned} \partial_t \langle \hat{\sigma}^z \rangle &= w(1 - \langle \hat{\sigma}^z \rangle) - \gamma - \langle \hat{\sigma}^z \rangle \gamma \zeta \\ &\quad - 2\gamma (\langle \hat{\sigma}_1^+ \hat{\sigma}_2^- \rangle (N - 1) + \xi N \text{Re} [\langle \hat{\sigma}_A^+ \hat{\sigma}_B^- \rangle]) \\ \partial_t \langle \hat{\sigma}_1^+ \hat{\sigma}_2^- \rangle &= \langle \hat{\sigma}_1^+ \hat{\sigma}_2^- \rangle (-w + \gamma(N - 2) \langle \hat{\sigma}^z \rangle - \gamma \zeta) \\ &\quad + \frac{\gamma}{2} \langle \hat{\sigma}^z \rangle (1 + \zeta \langle \hat{\sigma}^z \rangle + 2N\xi \text{Re} [\langle \hat{\sigma}_A^+ \hat{\sigma}_B^- \rangle]) \\ \partial_t \langle \hat{\sigma}_A^+ \hat{\sigma}_B^- \rangle &= \langle \hat{\sigma}_A^+ \hat{\sigma}_B^- \rangle (\gamma(N - 1) \langle \hat{\sigma}^z \rangle - \gamma \zeta - w + i\delta) \\ &\quad + \frac{\gamma}{2} \xi \langle \hat{\sigma}^z \rangle (2 \langle \hat{\sigma}^z \rangle \zeta (\xi^4 - \xi^2 + 2)^{-1} + 1) \\ &\quad + \gamma \xi \langle \hat{\sigma}^z \rangle \langle \hat{\sigma}_1^+ \hat{\sigma}_2^- \rangle (N - 1) \end{aligned} \quad (19)$$

with $\zeta := (\xi^4 - \xi^2 + 2) / (2(1 - \xi^2))$ and factorized $\langle \hat{\sigma}^z \rangle$ from all occurring correlation functions, giving a closed

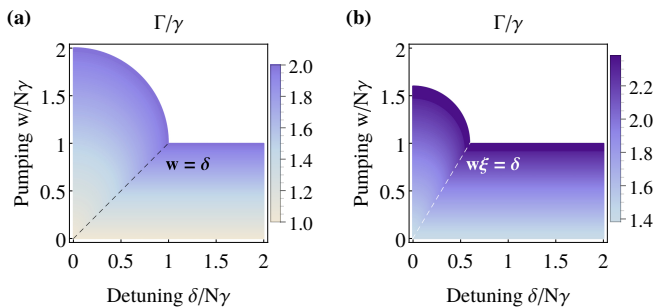


FIG. 11. The dimensionless linewidth Γ/γ for quantum (a) Eq. (6) and classical (b) Eq. (20) coupling with $\xi = 0.6$ for leading order in $1/N$. The linewidth for classical coupling (b) is always larger than the quantum coupling, due to noise term ζ increasing with coupling strength ξ . In the regime far above a critical pumping the atoms radiate chaotically [5] with a linewidth scaling with $O(N)$, which is not plotted here and typically many orders of magnitude larger than the linewidth in the superradiant regime.

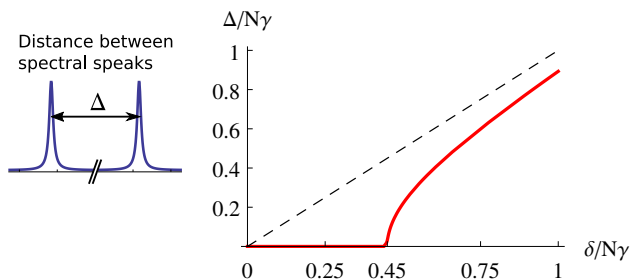


FIG. 12. Pole distance Δ of the output spectrum over the detuning δ with the critical detuning at $w\xi$, and the parameters $N\gamma = 10^6$ Hz, $w = 0.5N\gamma$, and $\xi = 0.9$. The dashed line is $\Delta = \delta$.

system of equations. We could use the same short notation for the expectation values as in Sec. II A, since the effective coupling in (17) is symmetric for both ensembles and even recover the equations of [9], when disregarding the relation between ζ and ξ and setting $\zeta = \xi = 1$. The steady state can now simply be calculated setting all time-derivatives equal to zero. These algebraic equations can be solved numerically or analytically, while filtering out the stable solution. Fig. 10 show the expectation values responsible for inter- and inner-ensemble correlations in the steady state and they are very similar to Fig. 3 in Section II A. The only difference is a by ξ reduced synchronization regime, visible in non-vanishing inter-ensemble correlations $\langle \hat{\sigma}_A^+ \hat{\sigma}_B^- \rangle$. The synchronized regime for leading order in $1/N$ is bounded by $w\xi = \delta$ and the quarter circle $(w - N\gamma)^2 + \delta^2 = (\xi N\gamma)^2$ (see Fig. 10a).

Analog to Section II A we can extract the half-width $\Gamma/2$ of the Lorentz peaks in the spectrum from the two-time correlation functions and use the analytical solution

for $\langle \hat{\sigma}^z \rangle$ (see (A.6)) up to leading order in $1/N$ to derive

$$\Gamma/\gamma = \zeta + \begin{cases} \frac{w - \sqrt{w^2 \xi^2 - \delta^2 (1 - \xi^2)}}{N\gamma(1 - \xi^2)}, & 0 \leq \delta < w\xi \\ \frac{w}{N\gamma}, & \delta \geq w\xi \end{cases}, \quad (20)$$

which is valid in the superradiant regime. This linewidth is plotted in Fig. 11b and compared with (6) from Section II A plotted in Fig. 11a. The linewidth using the classical coupling is larger than the linewidth using the quantum coupling, due to the measurement induced noise term ζ . This noise term ζ also prevents one to take the limit $\xi \rightarrow 1$ to approach the same synchronization regime as in Section II A, since ζ diverges in this limit.

The striking feature of the setup in Section II A was clear synchronization visible in the distance of the Lorentzian peaks Δ plotted over the bare detuning δ , which is also reproduced here with a smaller critical detuning $w\xi$ (see Fig. 12).

The results presented here show that the synchronization of superradiant lasers [9, 10] is not dominated by quantum effects, but a classical synchronization of quantum systems. However this classical coupling setup has a reduced synchronization regime and an increased linewidth, even with the ideal measurements and lasers assumed for the feedback. For any experimental realization the lasers for the feedback would need an even lower linewidth than the superradiant lasers. This setup is therefore of more theoretical interest to help defining the border between synchronization of quantum systems using classical channels and quantum systems using quantum channels.

IV. DISCUSSION

We discussed if and how synchronization occurs in a cascaded setup of master & slave superradiant atomic ensembles, or active atomic clocks. Additionally we simulated the symmetric coupling and the cascaded coupling with idealized classical coupling channels.

The cascaded setup in Section II B shows synchronization of the slave ensemble to the injected frequency. The main difference to Section II A is that the synchronization is not apparent in the distance Δ of the Lorentz peaks, but in the Lorentz peak heights. In the synchronized regime the slave ensemble radiates only at the injected frequency, while its Lorentz peak at the resonance frequency effectively vanishes.

In Section III A we replaced the direct injection of the light with a measurement and feedback, introducing a classical channel in between both cavities. The resulting steady state equations reveal only minor changes, which do not scale with the system size, resulting in basically identical steady state results and the same synchronization far above laser threshold.

ACKNOWLEDGMENTS

This work was funded by the Deutsche Forschungsgemeinschaft (DFG) in the research project RTG 1991 and through CRC 1227 (DQ-mat), project A05. We thank Hashem Zoubi and Jonas Lammers for fruitful discussions.

Appendix: Complete Derivation for the Bidirectional Synchronization using a Classical Channel

In this section we give a complete derivation of the results presented in Section III B. The system (see Fig. 9) is comprised out of two one-sided cavities, with decay rate $\tilde{\kappa}$ and are measured with ideal heterodyne measurements. The measurement results are then used by ideal lasers to recreate the measured coherent state with a certain gain. This can then be injected through the fully reflecting mirror by considering the limit of vanishing transmission and infinitely large laser gain resulting in a constant amplitude of the injected signal. Since measurement and feedback are symmetric, they realize a symmetric classical coupling channel between both cavities. To describe the system we use the unconditional feedback master equation (15) twice. Once with the measurement operator $\hat{s}_a = \sqrt{\tilde{\kappa}}\hat{a}$ with cavity decay rate $\tilde{\kappa}$ and feedback operators $\hat{F}_\pm^{\hat{b}} = g_\pm \hat{b} + g_\pm^* \hat{b}^\dagger$, and then with the measurement operator $\hat{s}_b = \sqrt{\tilde{\kappa}}\hat{b}$ and feedback operator $\hat{F}_\pm^{\hat{a}} = g_\pm \hat{a} + g_\pm^* \hat{a}^\dagger$, where $g_+ := g_-/i$. Without loss of generality we can define the feedback strength as $g_- := -\xi\sqrt{\tilde{\kappa}}$ with $\xi \in [0, \infty)$ giving the master equation in a rotating frame:

$$\begin{aligned} \dot{\rho} = & -i \left[\frac{\Omega}{2} \left(J_A^+ \hat{a} + J_B^+ \hat{b} + h.c. \right) + \frac{\delta}{2} (J_A^z - J_B^z), \rho \right] \\ & + w \sum_{\substack{T \in \{A,B\} \\ i \in \{1..N\}}} \mathcal{D} \left[\hat{\sigma}_{T,i}^+ \right] \rho + \tilde{\kappa} \mathcal{D} \left[\hat{a} + \xi \hat{b} \right] \rho + \xi^2 \tilde{\kappa} \mathcal{D} \left[\hat{b}^\dagger \right] \rho \\ & + \tilde{\kappa} \mathcal{D} \left[\hat{b} + \xi \hat{a} \right] \rho + \xi^2 \tilde{\kappa} \mathcal{D} \left[\hat{a}^\dagger \right] \rho. \end{aligned}$$

a. Stability

First it is important to recognize the stability regime of this feedback for the parameters $\tilde{\kappa}$ and ξ . One might think of the case where the feedback is effectively larger than the measurement result, giving in a net amplification and diverging amplitudes of the cavity fields. The dynamics of the expectation values

$$\frac{d}{dt} \begin{pmatrix} \langle \hat{a} \rangle \\ \langle \hat{b} \rangle \end{pmatrix} = -\frac{\tilde{\kappa}}{2} \begin{pmatrix} 1 & \xi \\ \xi & 1 \end{pmatrix} \begin{pmatrix} \langle \hat{a} \rangle \\ \langle \hat{b} \rangle \end{pmatrix} \quad (\text{A.1})$$

including only the fields is a stable system, if and only if all eigenvalues $-\frac{1}{2}\tilde{\kappa}(1 \pm \xi)$ are negative. This gives the stability condition $\xi < 1$. Furthermore (A.1) shows that

for $\xi = 0$ the fields \hat{a}, \hat{b} are completely decoupled, while for $\xi \lesssim 1$ the fields couple strongly.

b. Adiabatic Elimination

Using the reparameterization $\hat{c}_+ := (\hat{b} - \hat{a})/\sqrt{2}$ and $\hat{c}_- := (\hat{b} + \hat{a})/\sqrt{2}$ the Lindblad operators decouple and drive the fields \hat{c}_\pm into a thermal product state. Following the adiabatic elimination in this reparameterization we get the master equation for the atoms only

$$\begin{aligned} \dot{\rho} = & \frac{\delta}{2i} [J_A^z - J_B^z, \rho] + \sum_{\substack{T \in \{A,B\} \\ i \in \{1..N\}}} w \mathcal{D} \left[\hat{\sigma}_{T,i}^+ \right] \rho + \sum_{s=\pm} \frac{\Omega^2}{2\kappa_s} \times \\ & \times \left((1 + \bar{n}_s) \mathcal{D} [J_A^- - sJ_B^-] + \bar{n}_s \mathcal{D} [J_A^+ - sJ_B^+] \right) \rho, \end{aligned} \quad (\text{A.2})$$

where $\kappa_\pm := \tilde{\kappa}(1 \pm \xi)$ and $\bar{n}_\pm := \xi^2/(4(1 \pm \xi))$.

c. Coupling Parameterization

Two free parameters $\tilde{\kappa}$ and ξ remain in (A.2). We would like however to have one free parameter tuning between decoupled cavities and strongly coupled cavities simulating the setup in section II A. We can fix the remaining free parameter $\tilde{\kappa}$ using the dynamics of the expectation value

$$\begin{aligned} \frac{d}{dt} \langle \hat{\sigma}_A^+ \rangle = & \langle \hat{\sigma}_A^+ \rangle \sum_{s=\pm} \frac{\Omega^2}{4\kappa_s} ((N-1) \langle \hat{\sigma}^z \rangle - 1 - 2\bar{n}_s) \\ & + \langle \hat{\sigma}_A^+ \rangle \frac{i\delta - w}{2} - \langle \hat{\sigma}_B^+ \rangle \langle \hat{\sigma}^z \rangle N \sum_{s=\pm} \frac{s\Omega^2}{4\kappa_s}, \end{aligned} \quad (\text{A.3})$$

where we factorized the mean field $\langle \hat{\sigma}^z \rangle$, and compare it to the dynamics for uncoupled cavities and strongly coupled cavities as in Section II A.

Uncoupled, $\xi = 0$: (A.3) simplifies to:

$$\frac{d}{dt} \langle \hat{\sigma}_A^+ \rangle = \langle \hat{\sigma}_A^+ \rangle \left(\frac{\Omega^2}{\tilde{\kappa}} ((N-1) \langle \hat{\sigma}_A^z \rangle - 1) - w + i\delta \right) / 2$$

This can be compared to the top left matrix element of (11) in Sec. II B, since (11) is derived using the quantum regression theorem and holds identically also for the dynamics of $(\langle \hat{\sigma}_A^+ \rangle, \langle \hat{\sigma}_B^+ \rangle)^T$. Considering a shifted frequency detuning $\pm\delta/2$ restricts $\tilde{\kappa}(\xi = 0) = \kappa$.

Strongly coupled, $\xi \rightarrow 1$: The coefficients in (A.3) should be identical to the top left matrix element of (5) in Sec. II A for all variables scaling with the system size N . This gives the restriction for $\xi \rightarrow 1$:

$$\tilde{\kappa}(\xi) = \frac{\kappa}{2(1-\xi)}.$$

For ξ very close to unity the term not scaling with system size, $\langle \hat{\sigma}_A^+ \rangle \sum_{s=\pm} \frac{\Omega^2}{4\kappa_s} (-1 - 2\bar{n}_s)$, diverges and becomes dominant. This noise term grows $\propto (1 - \xi)^{-1}$ when ξ approaches the stability border and is negligible for completely decoupled systems and large N .

Medium coupling: Satisfying both extreme cases discussed before we can choose in between:

$$\tilde{\kappa}(\xi) := \frac{\kappa}{(1 - \xi)(1 + \xi)}. \quad (\text{A.4})$$

d. Steady State

From master equation (A.2) with the parameterization (A.4) we can calculate the dynamics of the expectation values of $\langle \hat{\sigma}^z \rangle$, $\langle \hat{\sigma}_1^+ \hat{\sigma}_2^- \rangle$, $\langle \hat{\sigma}_A^+ \hat{\sigma}_B^- \rangle$

$$\begin{aligned} \partial_t \langle \hat{\sigma}^z \rangle &= w(1 - \langle \hat{\sigma}^z \rangle) - \gamma - \langle \hat{\sigma}^z \rangle \gamma \zeta \\ &\quad - 2\gamma (\langle \hat{\sigma}_1^+ \hat{\sigma}_2^- \rangle (N - 1) + \xi N \text{Re} [\langle \hat{\sigma}_A^+ \hat{\sigma}_B^- \rangle]) \\ \partial_t \langle \hat{\sigma}_1^+ \hat{\sigma}_2^- \rangle &= \langle \hat{\sigma}_1^+ \hat{\sigma}_2^- \rangle (-w + \gamma(N - 2) \langle \hat{\sigma}^z \rangle - \gamma \zeta) \\ &\quad + \frac{\gamma}{2} \langle \hat{\sigma}^z \rangle (1 + \zeta \langle \hat{\sigma}^z \rangle + 2N\xi \text{Re} [\langle \hat{\sigma}_A^+ \hat{\sigma}_B^- \rangle]) \\ \partial_t \langle \hat{\sigma}_A^+ \hat{\sigma}_B^- \rangle &= \langle \hat{\sigma}_A^+ \hat{\sigma}_B^- \rangle (\gamma(N - 1) \langle \hat{\sigma}^z \rangle - \gamma \zeta - w + i\delta) \\ &\quad + \frac{\gamma}{2} \xi \langle \hat{\sigma}^z \rangle (2 \langle \hat{\sigma}^z \rangle \zeta (\xi^4 - \xi^2 + 2)^{-1} + 1) \\ &\quad + \gamma \xi \langle \hat{\sigma}^z \rangle \langle \hat{\sigma}_1^+ \hat{\sigma}_2^- \rangle (N - 1) \end{aligned} \quad (\text{A.5})$$

with $\zeta := (\xi^4 - \xi^2 + 2) / (2(1 - \xi^2))$ and factorized $\langle \hat{\sigma}^z \rangle$ from all occurring correlation functions, giving a closed system of equations. The steady state can now simply be calculated setting all time-derivatives equal to zero. These algebraic equations can be solved numerically or analytically, while filtering out the stable solution. One might try the limit $\xi \rightarrow 1$ to approach the coupling in

Section II A, only to discover that the term ζ , playing the role of a noise term, diverges. One recovers the equations of [9], when disregarding the relation between ζ and ξ and setting $\zeta = \xi = 1$, which shows that the quantum coupling has no inherent coupling noise.

e. Analysis and Comparison of the Peak Width

Analog to Section II A we can extract the information of the Lorentz peaks from the two-time correlation functions. They can be obtained by using (A.3) and the quantum regression theorem giving a differential equation system similar to (5), which can be easily solved. The two-time correlation functions consist out of linear combinations of exponential functions $\exp(-\frac{1}{2}(\Gamma_1 \pm x_1)\tau)$ with $x_1 = \sqrt{(\gamma N \xi \langle \hat{\sigma}^z \rangle)^2 - \delta^2}$ and $\Gamma_1 = w - \gamma(N - 1) \langle \hat{\sigma}^z \rangle + \gamma \zeta$. The width of the Lorentz curve is nothing else but the real part $\Gamma = \text{Re}[\Gamma_1 \pm x_1]$. To analyze the linewidth Γ we solve the system (A.5) up to leading order in $1/N$ giving:

$$\langle \hat{\sigma}^z \rangle = \begin{cases} \text{Min} \left(1, \frac{w - \sqrt{w^2 \xi^2 - \delta^2 (1 - \xi^2)}}{N \gamma (1 - \xi^2)} \right), & 0 \leq \delta < w \xi \\ \text{Min} \left(1, \frac{w}{N \gamma} \right), & \delta \geq w \xi \end{cases}. \quad (\text{A.6})$$

Plugging (A.6) back into $\Gamma = \text{Re}[\Gamma_1 \pm x_1]$ gives

$$\Gamma/\gamma = \zeta + \begin{cases} \frac{w - \sqrt{w^2 \xi^2 - \delta^2 (1 - \xi^2)}}{N \gamma (1 - \xi^2)}, & 0 \leq \delta < w \xi \\ \frac{w}{N \gamma}, & \delta \geq w \xi \end{cases},$$

which is valid in the superradiant regime, i.e. upper bounded by $\langle \hat{\sigma}^z \rangle < 1$ using (A.6).

For the plots of the relevant functions and their analysis we refer to Section III B.

-
- [1] T. Nicholson, S. Campbell, R. Hutson, G. Marti, B. Bloom, R. McNally, W. Zhang, M. Barrett, M. Safronova, G. Strouse, W. Tew, and J. Ye, *Nat Commun* **6**, (2015).
 - [2] A. D. Ludlow, M. M. Boyd, J. Ye, E. Peik, and P. O. Schmidt, *Rev. Mod. Phys.* **87**, 637701 (2015).
 - [3] A. Al-Masoudi, S. Dörscher, S. Häfner, U. Sterr, and C. Lisdat, *Phys. Rev. A* **92**, 063814 (2015).
 - [4] D. Meiser, J. Ye, D. R. Carlson, and M. J. Holland, *Physical Review Letters* **102**, 163601 (2009).
 - [5] D. Meiser and M. J. Holland, *Physical Review A* **81**, 063827 (2010).
 - [6] J. G. Bohnet, Z. Chen, J. M. Weiner, D. Meiser, M. J. Holland, and J. K. Thompson, *Nature* **484**, 78 (2012).
 - [7] J. G. Bohnet, Z. Chen, J. M. Weiner, K. C. Cox, and J. K. Thompson, *Physical Review A* **88**, 013826 (2013).
 - [8] M. A. Norcia, M. N. Winchester, J. R. K. Cline, and J. K. Thompson, *arXiv:1503.06464* (2016).
 - [9] M. Xu, D. A. Tieri, E. C. Fine, J. K. Thompson, and M. J. Holland, *Physical Review Letters* **113**, 154101 (2014).
 - [10] J. M. Weiner, K. C. Cox, J. G. Bohnet, and J. K. Thompson, *arXiv:1503.06464* (2015).
 - [11] P. Komar, E. M. Kessler, M. Bishof, L. Jiang, A. S. Sorensen, J. Ye, and M. D. Lukin, *Nat Phys* **10**, 582 (2014).
 - [12] O. V. Zhirov and D. L. Shepelyansky, *Physical Review B* **80**, 014519 (2009).
 - [13] T. E. Lee and H. R. Sadeghpour, *Physical Review Letters* **111**, 234101 (2013).
 - [14] A. Mari, A. Farace, N. Didier, V. Giovannetti, and R. Fazio, *Physical Review Letters* **111**, 103605 (2013).
 - [15] S. Walter, A. Nunnenkamp, and C. Bruder, *Physical Review Letters* **112**, 094102 (2014).
 - [16] T. E. Lee, C.-K. Chan, and S. Wang, *Physical Review E* **89**, 022913 (2014).

- [17] B. Zhu, J. Schachenmayer, M. Xu, F. Herrera, J. G. Restrepo, M. J. Holland, and A. M. Rey, *New Journal of Physics* **17**, 083063 (2015), arXiv: 1502.06055.
- [18] C. W. Gardiner and P. Zoller, *Quantum noise: a handbook of Markovian and non-Markovian quantum stochastic methods with applications to quantum optics* (Springer, Berlin; New York, 2004).
- [19] “QuTiP - Quantum Toolbox in Python,” (2015).
- [20] L. Mandel and E. Wolf, *Optical coherence and quantum optics* (Cambridge University Press, Cambridge, 1995).
- [21] S. G. Hofer, D. V. Vasilyev, M. Aspelmeyer, and K. Hammerer, *Physical Review Letters* **111**, 170404 (2013).
- [22] H. M. Wiseman and G. J. Milburn, *Physical Review Letters* **70**, 548 (1993).
- [23] “Quantum Mathematica Add-On by Jose Luis Gmez-Muoz,” (2016).